Journal of Building Engineering 42 (2021) 102795

Contents lists available at ScienceDirect

Journal of Building Engineering

journal homepage: www.elsevier.com/locate/jobe

# A comparative evaluation of semi-active control algorithms for real-time seismic protection of buildings via magnetorheological fluid dampers

Özge Şahin [a], Nurettin Gökhan Adar [b], Muaz Kemerli [c], Naci Çaglar [a,*], İsmail Şahin [e], Zekeriya Parlak [c], Salih Kükrek [d], Tahsin Engin [c]

[a] Department of Civil Engineering, Engineering Faculty, Sakarya University, 54187, Sakarya, Turkey
[b] Faculty of Engineering and Natural Sciences, Bursa Technical University, 16310, Bursa, Turkey
[c] Department of Mechanical Engineering, Engineering Faculty, Sakarya University, 54187, Sakarya, Turkey
[d] SANLAB Simulation, İstanbul, Turkey
[e] Vocational School of Akyazi, Sakarya University of Applied Sciences, Sakarya, Turkey

ARTICLE INFO

*Keywords:*
MR damper control
Semi-active control
Neural network
PID control
Sliding mode control
Shaking table test

ABSTRACT

Semi-active vibration control is considered a powerful method in reducing the dynamic responses of buildings by using additional smart damping devices. In this study, magnetorheological (MR) dampers have been proposed as one of the semi-active control devices to mitigate the structural vibrations and improve the seismic performance of the structures. The performance of the MR dampers strongly depends on implemented controllers. Hence, the main purpose of this paper is to evaluate the efficiency of several semi-active control algorithms related to MR dampers for seismic control of civil building structures. A 5-story test structure is manufactured, and an MR damper is installed between the ground and the first floor. The performance of the semi-active control approach is experimentally evaluated on a shaking table under historical earthquake records. A neural network-based modeling approach is adopted in the inverse MR damper model for the current control. Three different control algorithms, namely Proportional-Integral-Derivative (PID), Sliding Mode (SMC) and Energy-based controller (EBC), are applied to the system in real-time. The shaking tests are also carried out on the structures with different natural frequencies by increasing the number of stories without changing the geometry and material properties of the 5-story building model. The results indicate that the SMC controller is the most effective control algorithm among all controllers in reducing the base shear force by 51%.

## 1. Introduction

Earthquakes are one of the most destroying natural hazards, causing structural damage or collapse of buildings which may lead to the destruction of property and loss of life [1]. Protection of the structures subjected to seismic vibrations is one of the challenging tasks in civil engineering. Buildings are commonly designed as earthquake-resistant to prevent collapse under strong ground motions. However, the existing buildings also need to be strengthened in addition to the earthquake-resistant structural design. In this regard, complementary new approaches such as seismic energy damping systems have been proposed along with earthquake-resistant design. The use of various structural control systems in buildings to reduce seismic vibrations is one of the active research subjects [2]. Structural vibration control systems can be classified according to application methods as passive, active, semi-active and hybrid systems. The passive control systems doesn't require an input energy to operate, and the control forces are obtained based on the structural response [3,4]. The active control systems include actuators and require a large power source. These systems provide structural vibration control by imposing forces on a structure to counter-balance the seismic force [5–7]. The hybrid control system involves dampers and isolators together and uses the best

* Corresponding author.
*E-mail address:* caglar@sakarya.edu.tr (N. Çaglar).

https://doi.org/10.1016/j.jobe.2021.102795
Received 25 January 2021; Received in revised form 2 May 2021; Accepted 26 May 2021
Available online 1 June 2021

features of passive and active control systems [8]. The semi-active control system offers the reliability of the passive control systems and flexibility of the active control systems [9–11].

One of the most promising semi-active devices used in the control of structures is the magnetorheological (MR) damper that provides low control power, high force capacity, wide dynamic range, continuous adjustability and stability [12]. The excellent features make the MR damper is more attractive for practical application. Because of the nonlinear behavior of these energy dissipation devices, the practical realization of structural systems with MR dampers requires a suitable control algorithm. Researchers have designed numerous control algorithms ranging from a simple PID controller to advanced robust controllers to mitigate undesirable structural motion under seismic events. With respect to controllers of structures with MR dampers, an intelligent PID control algorithm is investigated for mitigating the structural vibrations of two-degrees of freedom system due to earthquake excitations and the results are compared with the H infinity controller case under the El Centro and Northridge earthquake inputs [13]. In Ref. [14], authors have proposed a clipped optimal control algorithm based on acceleration feedback to reduce structural vibrations of a scaled 3-story building under El Centro earthquake ground motion. The sliding mode control (SMC) is another commonly used controller [15,16]. The performance of the controller illustrated in Ref. [17]. The researchers has applied second-order SMC to the 3-story building model and compared the results with clipped optimal and Lyapunov-based controllers. Thus, the proposed controller has also been verified experimentally for a steel beam under sinusoidal ground excitation. In another study, researchers investigate the effectiveness of various algorithms to control a small-scale 6-story building with MR dampers on the lowest two floors utilizing Lyapunov controller, decentralized bang-bang controller, modulated homogeneous friction algorithm, clipped optimal controller and maximum energy dissipation algorithm [18]. In Ref. [19], the authors use the combination of the Linear quadratic regulator (LQR) and Artificial neural network (ANN) controller to evaluate the dynamic performance of a 6-story building for historical ground motions. Fuzzy logic controllers are also getting considerable attention in seismic control as a supplementary algorithm for parameter setting of other controllers or as a main controller. In Ref. [20], the investigation compares genetic-based fuzzy control and adaptive control algorithms for seismic protection of structures using MR dampers.

The objective of this study is to evaluate the performance of semi-actively controlled systems by different control algorithms that are not considered together in the literature before. The comparative evaluation of PID, sliding mode and energy-based controllers is performed according to the real-time experiments. The efficiency of the suggested control algorithms is experimentally investigated through the shaking table tests. Furthermore, the model structures with different natural frequencies are tested on scaled earthquake data to observe the MR damper performance at different amplitude levels. The damper is attached between the ground and the first floor of the building models. The inverse MR damper model based on the ANN algorithm is employed to predict the input current corresponding to the desired force. The experiments are carried out under two historical earthquakes, namely, (El Centro and Kocaeli). The model structures with different natural frequencies are designed by increasing the number of stories without changing the geometry and material properties of the 5-story steel building model. Illustration of the experimental results is made by using structural response data obtained from each algorithm and different performance criteria from the literature used for the comparison of the controllers. The paper is organized as follows: In Section 2, the design of the experimental building models, experimental measurement set-up, and control algorithms are presented with the inverse model of MR damper based on ANN. In Section 3, the experimental results are illustrated both numerically and graphically, along with a comparative discussion. Finally, the concluding remarks are drawn in Section 4.

The study has several limitations. 5-story test structure designed for the real-time experiments satisfies the dynamic similarity of the actual building with regard to frequency parameters except for geometry and material properties. It is assumed that the semi-actively controlled building responses remain in the linear elastic region, and a different solving strategy is required for the nonlinear structural control.

## 2. Methodology

This paper presents different semi-active control approaches applied to the structural systems equipped with an MR damper. PID, SMC and EBC controllers are used to obtain the desired damper force. The vibration reduction performances of the controllers are investigated experimentally. The general flow diagram illustrates the research steps followed in this study, given in Fig. 1.

### 2.1. Design of experimental building models

A 5-story reinforced concrete (RC) building is selected from the literature as a dynamic reference model of the 5-story steel building model shown in Fig. 2. In this study, the frequency characteristics of the RC building are considered in the test structure design.

The analytical, measured and updated frequencies of the real RC building are illustrated in Table 1. Further details can be found in the Ref. [21]. Since the seismic inputs are applied uniaxially (x-direction) to the test structures, the first and second updated mode frequencies of the RC building are selected as design parameters of the 5-story steel building model.

As shown in Table 2, the first and second mode frequencies demonstrate a good agreement between the real RC building and the 5-story steel building model.

The model structures used in the experiments are shown in Fig. 3. Each of the building models is supported by four steel columns which have rectangular section dimensions of 6 × 15 mm. The shorter dimension of the columns is aligned with the shaking direction of the excitation force. The height of the floors is 300 mm, and the columns are welded to the slab, each having size of 800 mm (long) x 600 mm (wide) x 15 mm (thickness).

The yield stress of the columns and the slab material are 750 MPa and 235 MPa, respectively. Bolts have been used to fix the base plate to the shaking table. Two tie bars are hinged between all of the floor slabs to minimize the horizontal motion (z-direction) of the model structures. Additional steel masses are added to each floor of the 5-story steel building model to match the natural frequency of the RC building given in Table 2. The model structures with different natural frequencies are constructed by increasing the number of stories without changing the geometry and material properties of the 5-story steel building model.

### 2.2. Experimental setup

The dynamic experiments were performed on a 6-DOF shaking table at the Sakarya University Earthquake Laboratory, shown in Fig. 4. The shaking table was manufactured by the Sanlab Simulation Inc., Turkey, with a plane of 2.5 m x 2.5 m and a maximum load capacity of 2000 kg.

The maximum displacement, velocity and acceleration of the

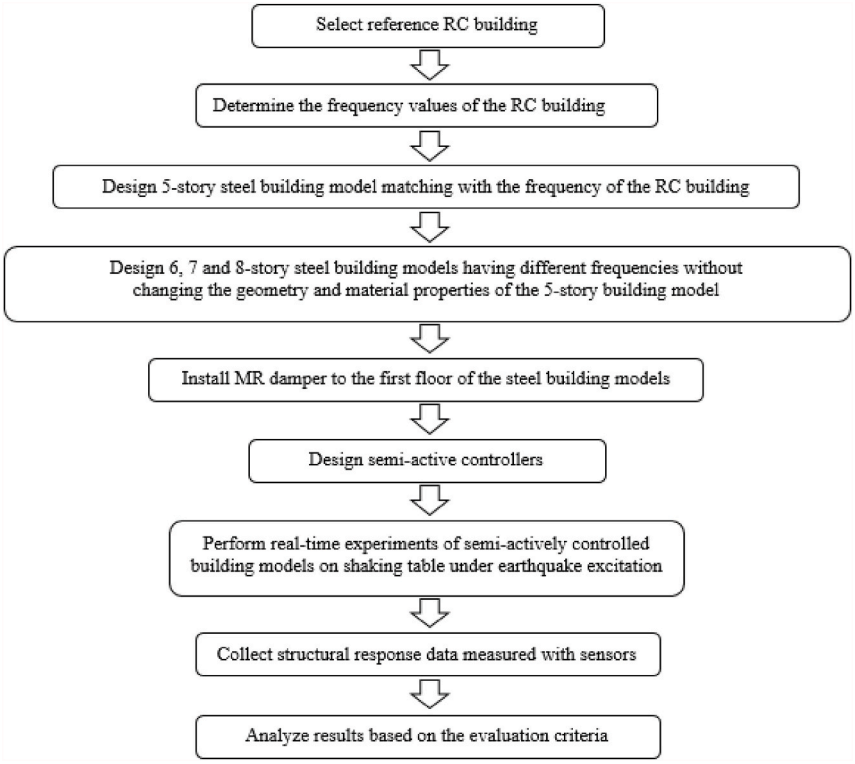


**Fig. 1.** Flow chart of research process.


**Fig. 2.** Proposed reinforced concrete building [21].

**Table 1**
Analytical, measured and updated frequencies of the reinforced concrete building (for only x-direction) [21].

| | Analytical Frequency (Hz) | Measured Frequency (Hz) | Updated Frequency (Hz) |
|---|---|---|---|
| First mode | 1.79 | 1.71 | 1.69 |
| Second mode | 5.28 | 5.63 | 5.23 |

**Table 2**
Frequency values of reference and model building (for only x-direction).

| | RC Building | Steel Building Model |
|---|---|---|
| | Updated Frequency (Hz) | Analytical Frequency (Hz) |
| First mode | 1.69 | 1.67 |
| Second mode | 5.23 | 4.88 |

shaking table are given in Table 3.

The floors of the model structures are equipped with SenseBox 7021 uniaxial and SenseBox 7023 triaxial acceleration transducers to monitor the dynamic responses of the test structures. The sensors are capable of receiving data with a sensitivity of 2400 mV/g within ± 3g range and can be used in seismic applications such as structural control, structural health monitoring, and modal analysis owing to their low noise and high resolution. Position transducers of UniMeasure placed on a rigid mast attached to the shaking table to measure the displacement response of the floors. Four displacement sensors are used in the experiments, and the position data of the interval floors are obtained by spline interpolation of the neighboring floors. LORD Inc. RD-8041-1 series MR damper, which has a maximum force capacity of around 2500 N, is placed in between the first floor and ground of the model structures (Fig. 4). The available stroke of the MR damper is 74 mm.

During the experiments, the excitation data of the El-Centro (USA, 1940) and Kocaeli (Turkey, 1999) earthquakes are applied to the shaking table as input ground motions (Fig. 5).

The model structures are excited with the scaled amplitudes of the

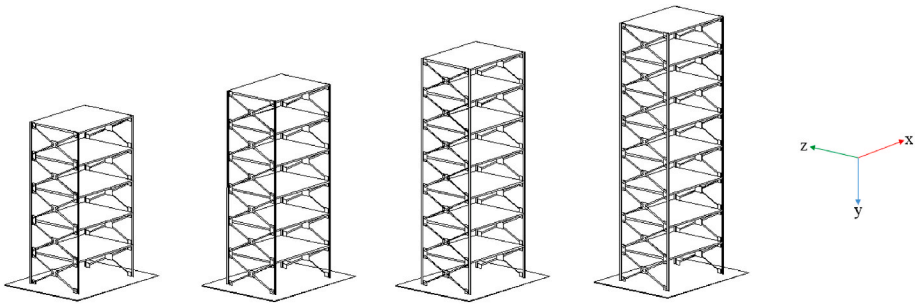


**Fig. 3.** Perspective views of the model structures.

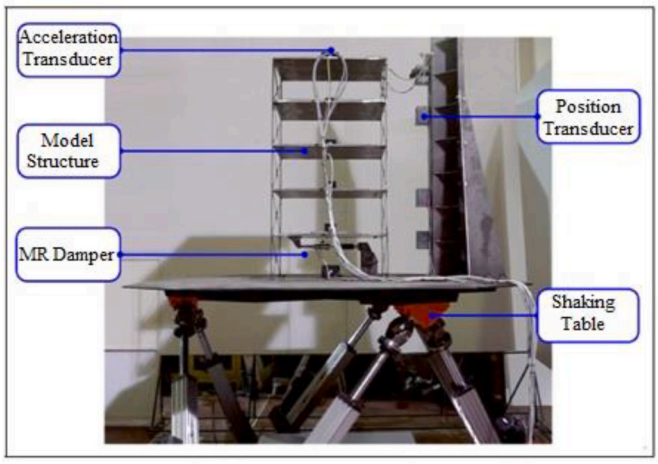


**Fig. 4.** Model structure and experimental setup.

**Table 3**
Maximum limits of the shaking table.

| | Displacement (m) | Velocity (m/s) | Acceleration (m/s$^2$) |
|---|---|---|---|
| **Surge (X)** | ±0.34 | ±0.7 | ±6 |
| **Sway (Y)** | ±0.33 | ±0.7 | ±6 |
| **Heave (Z)** | ±0.34 | ±0.55 | ±8 |

selected earthquakes in order to limit the maximum displacement responses to avoid structural damage (Table 4). To settle the fixed ended beam by a displacement $\Delta$ at one end, the required moment $M_z$ is expressed as follows:

$$M_z = \frac{6EI}{L^2}\Delta \tag{1}$$

where, $E$ is the modulus of elasticity, $I$ is the moment of inertia and $\Delta$ is the linear displacement of the beam [22].

The yield stress indicates the limit where a structural member begins to show an elastic behavior and can be defined as follows:

$$\sigma_{max} = \frac{M_z}{I} y \tag{2}$$

The maximum displacement value corresponding to the yield stress is obtained from Eq. (1) and Eq. (2). According to this approach, amplitudes of the earthquake ground motions are scaled to keep the response of the model structures in the linear elastic region.

### 2.3. Semi-active controllers

The control process of the MR damper consists of force and current control stages. The general block diagram of the semi-active control system is shown in Fig. 6. As illustrated in the figure, the system inputs are the earthquake excitation and damper force. In the force control stage, the required damper force is predicted by the controllers using the displacement, velocity and acceleration data measured from the model structures. In the current control stage, shown in the current controller block, the required current is predicted to obtain the desired force. The inverse MR damper model based on the ANN algorithm is used to obtain the input current applied to the MR damper.

Three control algorithms have been developed for force control which are PID control, sliding mode control and energy-based control.

#### 2.3.1. PID control

PID control is a prominent control algorithm with its easy structure and practical implementation in real-time. A general mathematical expression of PID control is given as follows:

**Table 4**
Scaling coefficients of earthquake accelerations applied to building models.

| Earthquake Data | Scale Coefficient | | | |
|---|---|---|---|---|
| | 5-Story | 6-Story | 7-Story | 8-Story |
| El-Centro,1940 | 1.0 | 0.7 | 0.4 | 0.3 |
| Kocaeli,1999 | 0.5 | 0.4 | 0.4 | 0.4 |

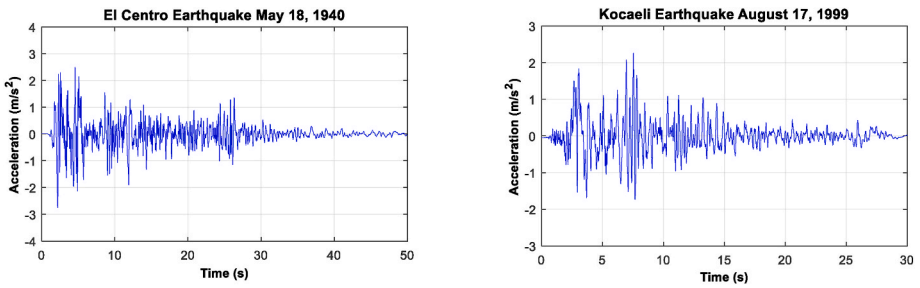


**Fig. 5.** Time history of earthquake accelerations used in experiments.

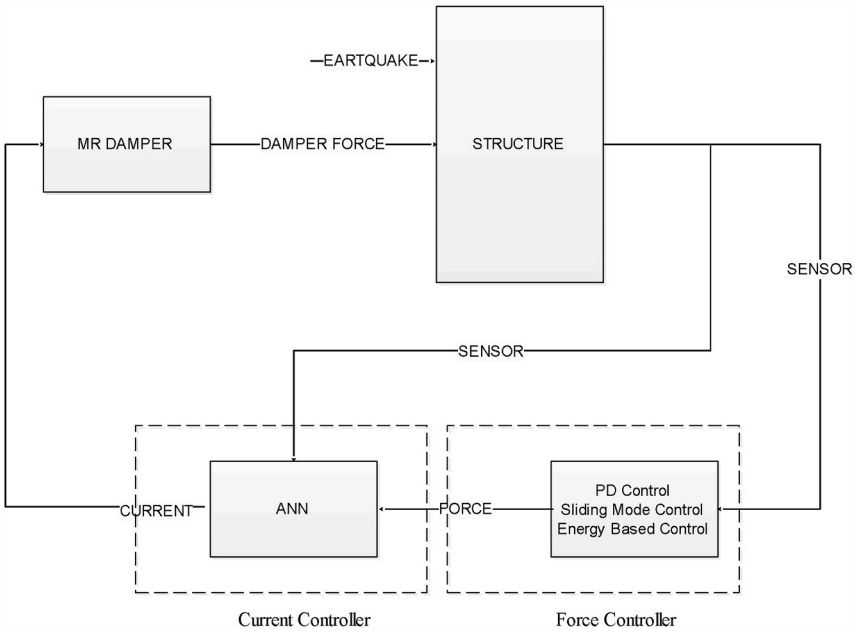


**Fig. 6.** Block diagram of the system.

$$u = K_p e + K_i \int_0^t e dt + K_d \frac{de}{dt} \tag{3}$$

where, $u$ is control signal, $e$ is error and $K_p$, $K_i$, and $K_d$ are the coefficients of the proportional, integral, and derivative terms, respectively.

The velocity of the floor is selected as feedback. In this case, the error becomes:

$$e = v_{ref} - v_1 \tag{4}$$

where, $v_{ref}$ is the reference velocity of the floor where the damper is connected and $v_1$ is the actual velocity of the floor.

During the earthquake, the building velocity response is aimed to be zero, which means a regulator control system is applied ($v_{ref} = 0$). Therefore, the obtained error can be expressed as follows:

$$v_{ref} = 0 \rightarrow e = -v_1 \tag{5}$$

The integral control is not used due to the random and instant peaks observed in the earthquake signals, and the PID controller will be called as PD controller hereafter. If $e = v_1$ and $u = f$ in Equations (3)–(5), then the desired force from the MR damper can be obtained as follows:

$$f_{damper} = -\left[K_p v_1 + K_d \frac{dv_1}{dt}\right] \tag{6}$$

The trial and error method is used to determine the optimum coefficients, considering the evaluation criteria given in Table 9. To determine the controller coefficients of PD, P is set to 3000 and increased with an increment of 2000. After every test, the six control criteria are evaluated, and the optimum P-value is decided. After the determination of P, the D coefficient is increased from 0 with an increment of 50. The optimum value of the controller is determined with PD coefficients where the best performance is obtained regarding the evaluation criteria. The optimum values used as the control coefficients of $K_p$ and $K_d$ are given in Table 5.

**Table 5**
PD coefficients.

| Steel Building Models | Earthquake Type | $K_p$ | $K_D$ |
|---|---|---|---|
| 5-Story | El-Centro | 3000 | 100 |
| | Kocaeli | 3000 | 50 |
| 6-Story | El-Centro | 7000 | 100 |
| | Kocaeli | 5000 | 150 |
| 7-Story | El-Centro | 7000 | 200 |
| | Kocaeli | 7000 | 50 |
| 8-Story | El-Centro | 10000 | 200 |
| | Kocaeli | 10000 | 200 |

### 2.3.2. Sliding mode control

In the sliding mode control (SMC), it is intended to bring the system output to the desired reference signal along a sliding surface and to keep the system output at the desired value by switching the control input. Further information about SMC can be found in the reference [16].

Displacement and velocity of the floor where the MR damper is connected are used as control feedback. The error between the reference and actual position and between the reference and actual velocity can be represented in the following vector form:

$$e = \begin{bmatrix} \Delta x \\ \Delta v \end{bmatrix} = \begin{bmatrix} x_{ref} - x_{act} \\ v_{ref} - v_{act} \end{bmatrix} \tag{7}$$

Since the displacement and the velocity of the building during the earthquake are desired to be zero ($x_{ref} = 0$ and $v_{ref} = 0$), the error can be written as follows:

$$e = \begin{bmatrix} \Delta x \\ \Delta v \end{bmatrix} = \begin{bmatrix} 0 - x_{act} \\ 0 - v_{act} \end{bmatrix} \tag{8}$$

Regarding to the approach in the literature [16], the sliding surface can be defined as:

$$\sigma = G\xi = [\alpha \quad \beta] \begin{bmatrix} \Delta x \\ \Delta v \end{bmatrix} \tag{9}$$

where, $\alpha$ and $\beta$ stand for the weight of displacement and velocity error, respectively.

In order to enforce finite time convergence for the system, $\sigma$ should satisfy the following:

$$\dot{\sigma} + \lambda\sigma + \mu sign(\sigma) = 0 \tag{10}$$

where $\lambda$ is the Lyapunov stability condition, $\sigma$ is sliding manifold and $\dot{\sigma}$ is the derivative of the sliding manifold.

The derivative of the sliding manifold can be expressed as follows:

**Table 6**
Sliding mode control coefficients of $\alpha$, $\beta$ and $\lambda$

| Steel Building Models | Earthquake Type | $\alpha$ | $\beta$ | $\lambda$ |
|---|---|---|---|---|
| 5-Story | El-Centro | 1 | 3 | 5000 |
| | Kocaeli | 1 | 3 | 5000 |
| 6-Story | El-Centro | 10 | 10 | 20000 |
| | Kocaeli | 5 | 5 | 15000 |
| 7-Story | El-Centro | 1 | 5 | 10000 |
| | Kocaeli | 1 | 5 | 10000 |
| 8-Story | El-Centro | 1 | 7 | 10000 |
| | Kocaeli | 1 | 7 | 10000 |

$$\dot{\sigma} = GB(u^{eq} - u) \tag{11}$$

Using Eqs. (10) and (11), the force required for the MR damper is obtained in discrete-time as follows:

$$f[k] = f[k-1] + (GB)^{-1}(\lambda\sigma + \mu sign(\sigma)) \tag{12}$$

where, *f [k]* and *f [k−1]* stand for the desired force of the current and previous step of the real-time control algorithm, respectively.

To determine the coefficients of SMC, first, the optimum point of $\lambda$ is searched by increasing the value from 3000 with an increment of 2000 or 3000. After determining the optimum $\lambda$ point, $\beta$ is increased from 1 with an increment of 2. $\alpha$ is kept constant at 1. The optimum values used as the control coefficients based on the evaluation criteria are given in Table 6.

### 2.3.3. Energy-based control

It is well-known that during an earthquake, a building experiences an accelerating motion. This causes each floor to accelerate and lead to an increase in the total kinetic energy of the building. To avoid this, a control algorithm based on energy optimization is designed considering the total increase in kinetic energy and optimize the total kinetic energy during the earthquake. The total kinetic energy of the building can be expressed as:

$$E_{total} = \sum_{i=1}^{n}\left(\frac{1}{2}m_i v_i(t)^2\right) \tag{13}$$

where, $m_i$, $v_i$ and $E_{total}$ stand for the effective mass of the $i_{th}$ floor, the velocity of the $i_{th}$ floor and the total kinetic energy of the floors, respectively.

The expression for the control algorithm is defined as follows:

$$f_{damper} = K\frac{E_{total}}{E_{max}} \tag{14}$$

where, $E_{max}$ is the maximum energy of the structure and $K$ is the control coefficient.

To determine the suitable control coefficient, $K$ is increased from a value around 5 (which is defined depending on the model building) with an increment of 2 or 3. The selected values for the control coefficient $K$ providing the best performance according to the evaluation criteria are given in Table 7.

**Table 7**
Energy-based control coefficient.

| Steel Building Model | Earthquake Type | K |
|---|---|---|
| 5-Story | El-Centro | 8 |
| | Kocaeli | 16 |
| 6-Story | El-Centro | 15 |
| | Kocaeli | 10 |
| 7-Story | El-Centro | 15 |
| | Kocaeli | 15 |
| 8-Story | El-Centro | 15 |
| | Kocaeli | 5 |

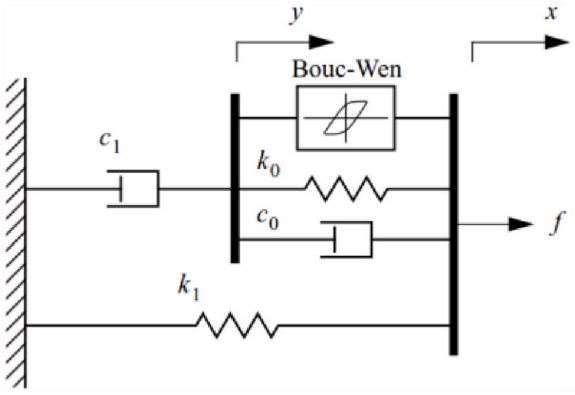


**Fig. 7.** Schematic representation of MR damper Bouc-Wen model [14].

### 2.4. Current controller (inverse MR damper modelling)

In order to create the desired force, the current value fed to the MR damper should be defined precisely. To realize this, an inverse MR damper model should be created.

Different mathematical models of MR damper are proposed in the literature. Bouc-Wen is the most widely used mathematical model, and the schematic representation is shown in Fig. 7 [14].

The mathematical equation of the Bouc-Wen model is as follows:

$$f = az + c_o(\dot{x} - \dot{y}) + k_o(x - y) + k_1(x - x_o) \tag{15}$$

where, $\alpha$, $k_0$ and $c_0$ stand for Bouc-Wen model coefficient, spring stiffness and dashpot damping coefficient of the MR damper, respectively. In equation (15), z represents the hysteretic deformation and given by the following equation:

$$\dot{z} = -\gamma|(\dot{x} - \dot{y})||z|^{n-1} - \beta|(\dot{x} - \dot{y})||z|^{n} + A|(\dot{x} - \dot{y})| \tag{16}$$

where $A$, $\gamma$, and $\beta$ are the parameters of the hysteretic model.

The above mathematical model is not suitable for real-time applications due to its highly nonlinear structure and difficulties in transforming it into an inverse model. Therefore, Artificial Neural Network (ANN) model was used for the inverse modeling of the MR damper in this study.

### 2.4.1. Inverse ANN model of the MR damper

In the study, the predicted force values should be converted to the input current of the MR damper, which requires an inverse MR damper model. In the literature, it is easy to find a forward model for the MR damper. Bouc-Wen model presented above is the most common forward model, and various parametric models are proposed for MR dampers, such as Dahl friction model [23] or Lu-Gre friction model [24]. Algebraic models also exist in the literature proposed by Kwok [25] or Guo [26]. However, to the authors' knowledge, there are very few parametric inverse models of MR damper due to the non-linearity and hysteretic behavior of the MR damper. For example, the most common Bouc-Wen model is very hard to be applied as an inverse model [27]. Thus, non-parametric methods become prominent such as fuzzy logic [28] and ANN model [29]. Therefore, an inverse ANN model has been adopted in the study. ANN is a commonly used method to obtain inverse and forward modeling of the MR dampers [30–34]. The required current to generate the desired force is calculated by considering the velocity and the displacement of the MR damper, which corresponds to a 3 input, 1 output ANN model.

The data required for the training of ANN was obtained from the performance tests of the MR damper. In this data set, the inputs of the ANN are the displacement, the velocity and the force of the MR damper. The output of the ANN is the input current of the MR damper. In order to model the hysteretic behavior of the MR damper, 2 previous steps of

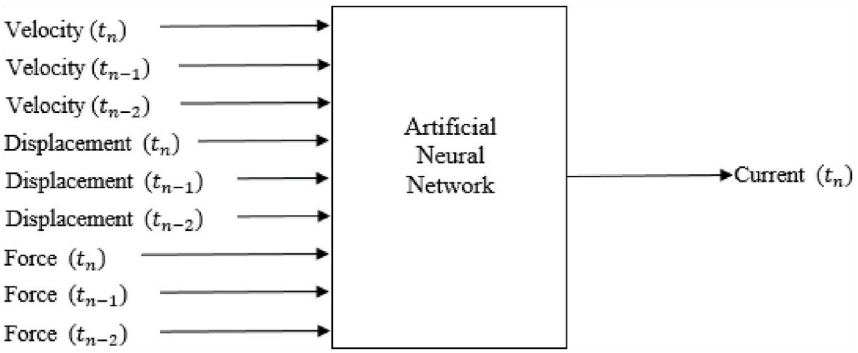


**Fig. 8.** Graphical representation of a neural network.

**Table 8**
Properties of the artificial neural network.

| ANN model | Number |
|---|---|
| Hidden Neuron Layers | 3 |
| Number of Neurons in the first layer | 10 |
| Number of Neurons in the second layer | 10 |
| Number of Input Neurons | 9 |
| Number of Output Neurons | 1 |
| Sampling Number | 16712 |

**Table 9**
Summary of evaluation criteria for the second generation benchmark problem.

| | |
|---|---|
| Interstory Drift Ratio $J_1 = max\left[\frac{max_{t,i}\lvert d_i(t)\rvert}{\delta^{max}}\right]$ | Normed Interstory Drift Ratio $J_4 = max\left[\frac{max_i d_i(t)}{\delta^{max}}\right]$ |
| Level Acceleration $J_2 = max\left[\frac{max_{t,i}\lvert \ddot{x}_{ai}(t)\rvert}{\ddot{x}_a^{max}}\right]$ | Normed Level Acceleration $J_5 = max\left[\frac{max_i \ddot{x}_{ai}(t)}{\ddot{x}_a^{max}}\right]$ |
| Base Shear $J_3 = \left[\frac{max\lvert k_1 \cdot x_1(t)\rvert}{\lvert F_b^{max}\rvert}\right]$ | Normed Base Shear $J_6 = \left[\frac{max\lvert k_1 \cdot x_1(t)\rvert}{F_b^{max}}\right]$ |

displacement, velocity and force values $(t_{n-1}, t_{n-2})$ are also considered in the model, which makes 9 inputs in total and presented in Fig. 8.

The structure of the ANN algorithm was optimized by trial-error method by using a similar dataset, and 3 hidden layers with 10 neurons of each are decided as the final structure which showed the best performance. Levenberg-Marquardt method was used in the training of the ANN model, which is the most common second-order training method of ANN and can handle more complex problems while retaining compact network sizes [35]. 80% of the data was used for training, while the remaining 20% used for the tests. The input data has been scaled between −1 and 1 and the output data has been scaled between 0 and 1 since the output current having positive values. The calculations were made primarily via MATLAB and then transferred to an in-house software interface via QT and Visual Studio. The properties of the ANN are given in Table 8.

The performance tests of the MR damper were conducted in Sakarya University Mechanical Engineering Applied Fluid Mechanics laboratory with Roehrig MK-2150 test device equipped with a 22 kN load cell and an LVDT sensor. A current sweep was applied to capture the behavior of the MR damper depending on the applied current, which start from 0 A to 1 A with an increment of 0.1 A and from 1 A to 2 A with an increment of 0.5 A. Velocity, displacement and force values were recorded by SHOCK 6.3 software for each corresponding current value to create the ANN training data. The temperature was kept constant at 20 °C by a temperature bath since the force output of MR damper is temperature-dependent.

## 3. Experimental results and discussion

To demonstrate the effectiveness of semi-active controllers, a series of shaking table experiments were conducted on 5-8 story building models. The model structures were subjected to scaled versions of the El-Centro and Kocaeli earthquakes. The acceleration and displacement response of the floors were recorded. PID, sliding mode and energy-based controllers were used to control the MR damper. These controllers were optimized by the trial-error method described in previous sections.

To compare the performance of the proposed control algorithms, the result of the passive-off case (no current applied to MR damper) is utilized. The displacement time history responses of different control algorithms for the first floor of the 5-story steel building model are shown in Fig. 9. It is clearly seen that implemented control algorithms reduce the displacement response of the model structure compared to the passive-off case in different earthquake excitations.

On the other hand, Figs. 10–13 illustrate the peak interstory drift responses of the 5 to 8-story model structures utilizing the implemented control algorithms.

The model structures used herein have different natural frequencies, which means they are affected differently by the earthquake vibration. For this reason, the model structures considered in this study are evaluated separately for each controller. First, the 5-story steel building model is considered in Fig. 10, and it is shown the peak interstory drift at the first floor of the structure is reduced significantly by the SMC algorithm, but it is not effective on the upper floors. PD and EBC algorithms are more effective in reducing the drift throughout the structure. Considering the responses shown by the 6-story steel building model in Fig. 11, the peak interstory drift of the first floor is reduced effectively by SMC and PD algorithms under El-Centro and Kocaeli earthquakes, respectively. However, EBC algorithm achieves higher performance than all of the other algorithms in reducing the interstory drift throughout the structure. Considering the 7 and 8-story steel building models, the maximum interstory drift is slightly less than that of the passive-off control (Figs. 12 and 13). Implemented control algorithms achieve very close performance levels under the El-Centro earthquake. EBC algorithm appears to be slightly more effective in reducing the drifts of lower floors under the Kocaeli earthquake.

In addition to the plots above, the structural responses obtained in real-time were evaluated numerically. For this purpose, six evaluation criteria ($J_1$-$J_6$), which are commonly used in the literature [36], are selected. The summary of these performance indexes for the second generation benchmark problem is presented in Table 9. Here, $J_1$, $J_2$, $J_3$ represent the maximum value of the interstory drift, floor accelerations and base shear force, while $J_4$, $J_5$, $J_6$ represent the normed interstory

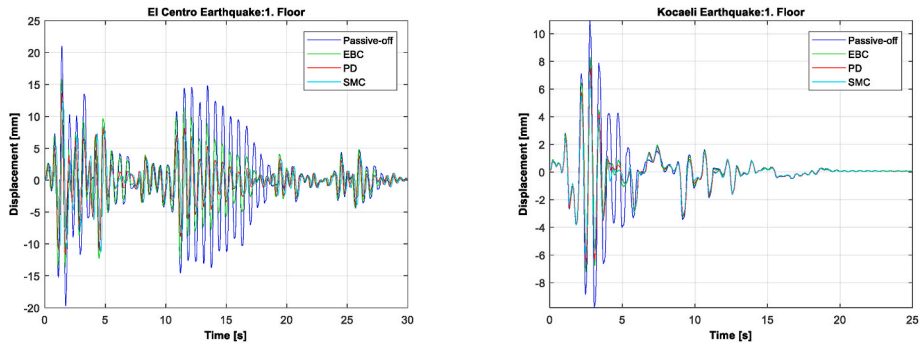


**Fig. 9.** Passive-off and semi-actively controlled displacement time histories of the 5-story structure under the El-Centro and Kocaeli earthquakes.

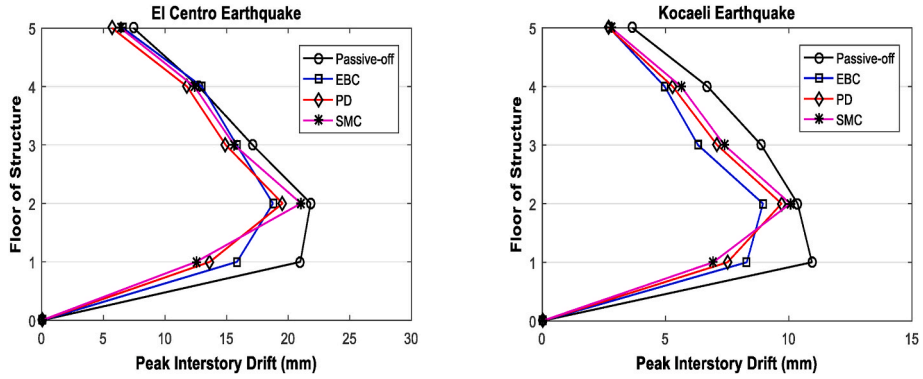


**Fig. 10.** Peak Interstory drift responses of each floor of 5-story steel building model (left:El-Centro Earthquake right:Kocaeli Earthquake).

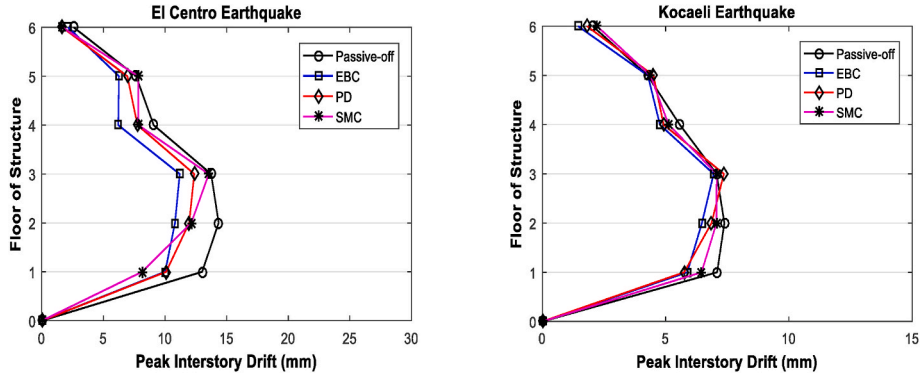


**Fig. 11.** Peak Interstory drift responses of each floor of 6-story steel building model (left:El-Centro Earthquake right:Kocaeli Earthquake).

drift, normed floor acceleration and normed base shear force, respectively.

Table 10 illustrates the peak and normed responses of the uncontrolled (passive-off) and PD, SMC, and EBC controlled model structures based on the evaluation criteria.

The PD controller achieves higher performance levels than that of the passive-off system based on $J_1$ and $J_4$ evaluation criteria. The maximum reduction in the peak and normed interstory drift ratio are 22% and 25%, respectively. However, this controller causes a significant increase in the peak acceleration level ($J_2$). The PD controller also achieves a 21% maximum reduction in the normed acceleration ($J_5$), and it demonstrates the best performance in reducing the base shear force at the high amplitude levels of the earthquakes. The maximum peak and normed base shear ($J_3$ and $J_6$) are reduced down to 35% and 49%, respectively.

The sliding mode controller exhibits lower performance levels than that of the passive-off case considering ($J_1$,$J_2$ and $J_4$) evaluation criteria. The maximum reduction in the peak and normed interstory drift ratio are 18% and 21%, respectively, and this controller achieves a maximum reduction of 13% in the normed acceleration level ($J_5$). The maximum peak and normed base shear ($J_3$ and $J_6$) are reduced down to 41% and 51%, respectively.

The energy-based controller achieves a similar performance level with the passive-off case in reducing the maximum interstory drift indicated with ($J_1$) evaluation criteria. The maximum reduction observed in the peak interstory drift ratio is 22%. The maximum normed interstory drift ratio is reduced down to 23%. The performance of this controller is very poor in reducing the acceleration response. The peak acceleration level ($J_2$) is increased up to 54% at high amplitude levels of the excitations. The controller also achieves only an 11% maximum reduction in the normed acceleration ($J_5$). The maximum peak and

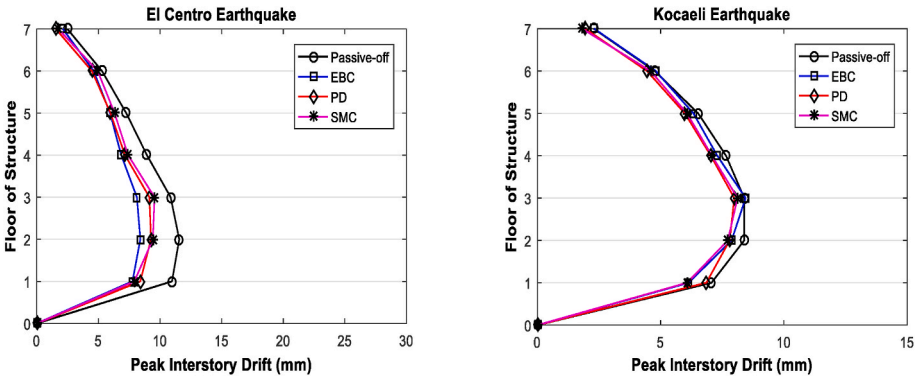


**Fig. 12.** Peak Interstory drift responses of each floor of 7-story steel building model (left:El-Centro Earthquake right:Kocaeli Earthquake).

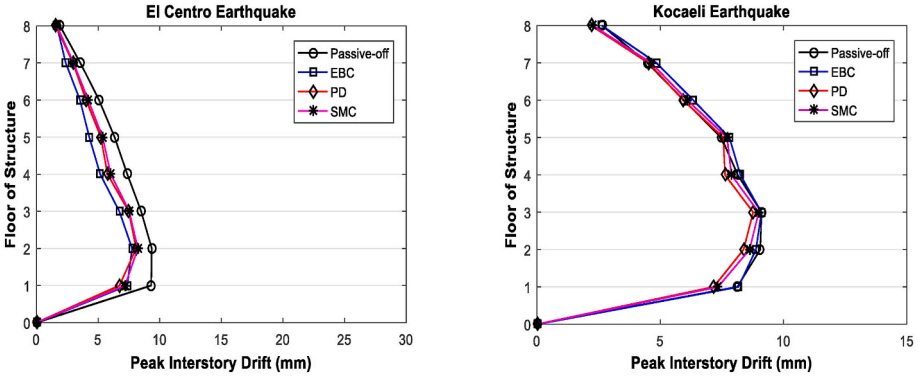


**Fig. 13.** Peak Interstory drift responses of each floor of 8-story steel building model (left:El-Centro Earthquake right:Kocaeli Earthquake).

**Table 10**
Evaluation criteria for the uncontrolled (passive-off) and PD, SMC, EBC controlled model structures.

| 5-Story Building | El-Centro Earthquake | | | | | | Kocaeli Earthquake | | | | | |
|---|---|---|---|---|---|---|---|---|---|---|---|---|
| | $J_1$ | $J_2$ | $J_3$ | $J_4$ | $J_5$ | $J_6$ | $J_1$ | $J_2$ | $J_3$ | $J_4$ | $J_5$ | $J_6$ |
| Passive-off | 1.00 | 1.00 | 1.00 | 1.00 | 1.00 | 1.00 | 1.00 | 1.00 | 1.00 | 1.00 | 1.00 | 1.00 |
| PD | 0.92 | 1.34 | 0.65 | 0.75 | 0.79 | 0.51 | 0.84 | 0.93 | 0.68 | 0.83 | 0.87 | 0.64 |
| SMC | 0.97 | 1.01 | 0.59 | 0.79 | 0.87 | 0.49 | 0.88 | 0.94 | 0.63 | 0.87 | 0.89 | 0.60 |
| EBC | 1.02 | 1.54 | 0.75 | 0.77 | 0.91 | 0.68 | 0.78 | 1.17 | 0.75 | 0.77 | 0.89 | 0.67 |
| **6-Story Building** | El-Centro Earthquake | | | | | | Kocaeli Earthquake | | | | | |
| | $J_1$ | $J_2$ | $J_3$ | $J_4$ | $J_5$ | $J_6$ | $J_1$ | $J_2$ | $J_3$ | $J_4$ | $J_5$ | $J_6$ |
| Passive-off | 1.00 | 1.00 | 1.00 | 1.00 | 1.00 | 1.00 | 1.00 | 1.00 | 1.00 | 1.00 | 1.00 | 1.00 |
| PD | 0.94 | 1.13 | 0.77 | 0.91 | 0.95 | 0.70 | 1.05 | 1.44 | 0.81 | 0.97 | 0.97 | 0.82 |
| SMC | 1.04 | 1.28 | 0.62 | 1.00 | 0.97 | 0.59 | 1.04 | 1.12 | 0.91 | 0.97 | 0.98 | 0.92 |
| EBC | 1.02 | 1.23 | 0.76 | 0.87 | 0.98 | 0.67 | 0.98 | 1.13 | 0.82 | 0.93 | 0.95 | 0.81 |
| **7-Story Building** | El-Centro Earthquake | | | | | | Kocaeli Earthquake | | | | | |
| | $J_1$ | $J_2$ | $J_3$ | $J_4$ | $J_5$ | $J_6$ | $J_1$ | $J_2$ | $J_3$ | $J_4$ | $J_5$ | $J_6$ |
| Passive-off | 1.00 | 1.00 | 1.00 | 1.00 | 1.00 | 1.00 | 1.00 | 1.00 | 1.00 | 1.00 | 1.00 | 1.00 |
| PD | 0.78 | 1.14 | 0.76 | 0.85 | 0.90 | 0.72 | 0.94 | 0.95 | 0.93 | 0.99 | 0.98 | 0.87 |
| SMC | 0.82 | 0.98 | 0.72 | 0.88 | 0.91 | 0.68 | 0.97 | 1.04 | 0.86 | 0.99 | 1.00 | 0.83 |
| EBC | 0.85 | 1.21 | 0.71 | 0.79 | 0.89 | 0.65 | 1.00 | 1.14 | 0.86 | 0.94 | 1.00 | 0.83 |
| **8-Story Building** | El-Centro Earthquake | | | | | | Kocaeli Earthquake | | | | | |
| | $J_1$ | $J_2$ | $J_3$ | $J_4$ | $J_5$ | $J_6$ | $J_1$ | $J_2$ | $J_3$ | $J_4$ | $J_5$ | $J_6$ |
| Passive-off | 1.00 | 1.00 | 1.00 | 1.00 | 1.00 | 1.00 | 1.00 | 1.00 | 1.00 | 1.00 | 1.00 | 1.00 |
| PD | 0.89 | 1.03 | 0.72 | 0.96 | 1.01 | 0.73 | 1.01 | 1.23 | 0.88 | 0.86 | 0.89 | 0.69 |
| SMC | 0.87 | 0.97 | 0.77 | 0.99 | 0.99 | 0.77 | 1.03 | 1.08 | 0.90 | 0.89 | 0.92 | 0.76 |
| EBC | 0.91 | 0.99 | 0.79 | 0.93 | 1.04 | 0.76 | 1.07 | 1.06 | 1.00 | 0.97 | 0.98 | 0.97 |

normed base shear ($J_3$ and $J_6$) are reduced down to 29% and 35%, respectively.

Considering the behavior of the buildings under seismic loads, the most important parameter among the evaluation criteria is the base shear force ($J_3$ and $J_6$). The maximum expected lateral force at the base of structures due to seismic loads is determined by the base shear force. As outlined in ASCE 7–10, the method used to develop equivalent static lateral loads on a structure that considers the effect of horizontal earthquake accelerations is called the Equivalent Lateral Force Procedure (ELFP). ASCE 7–10 Section 12.8 describes the seismic base shear

force determined by the Equivalent Lateral Force Procedure [37]. The energy transferred to structures is also related to the base shear force. The reduction in $J_3$ index is critical for the potential deterioration of the material, and a smaller $J_6$ index means a decreased fatigue on building elements. According to $J_3$ and $J_6$ indices, the smallest base shear force is achieved with the SMC algorithm on the 5 and 6-story steel building models. On the other hand, PD is the most effective algorithm in reducing the base shear force for 7 and 8-story steel building models.

## 4. Conclusion

In this paper, the effectiveness of three different semi-active control algorithms in structural systems using MR damper has been evaluated together. The controllers, namely PID, sliding mode and energy-based controller, are investigated with real-time shaking table tests of model structures having different stories. The structural responses under the scaled earthquake excitations are discussed for each control algorithm experimentally. The MR damper is placed on the first floor of the building models, and the control algorithms use the measurements obtained from position and acceleration sensors located on floors. The passive-off case (no current is applied to MR damper) is used as a reference to compare the performance of the proposed control algorithms.

The following concluding remarks can be drawn:

- Considering the structural performance, controllers achieved a similar performance level in reducing the $J_1$ and $J_4$ index. The maximum peak and normed interstory drift ratio are reduced to 18–22% and 21–25%, respectively.
- The semi-active controllers showed a significant reduction in $J_5$, time-averaged acceleration level, by %11–21, although the maximum acceleration level, $J_2$, is slightly increased. It has been observed that reducing the displacement responses triggers higher accelerations.
- Considering the performance objective to minimize $J_3$ and $J_6$ index, SMC is the most effective control algorithm among all controllers in reducing the base shear force by 41% and 51%, respectively.
- Each of the applied semi-active control algorithms achieved an improvement in structural performance over the passive-off control, although the performance varies depending on the implemented control algorithm.
- PID controller generally showed poor performance due to the highly nonlinear structure of the MR damper.
- Proposed control algorithms demonstrated the best performance levels on the 5-story steel building responses. The control forces at low amplitude scaled excitations are relatively small and have a slight effect on the responses of 6 to 8-story model structures.

Although a specific controller may achieve better performance for some structures, it may not work well for other systems. This indicates that the performance of the control algorithms depends on the structural system and applied earthquake data. It is necessary to compare the structural responses by using ground motions with the same hazard level. The efficacy of the controller on the first floor decreases when increasing the story of the buildings, and it can only be successful on the lower floors. Thus, the optimum number and location of dampers depending on the structures need to be investigated. To obtain a better performance evaluation for the semi-actively controlled structures with MR dampers, it is essential to increase the number of seismic ground motions, building models and control algorithms.

## Declaration of competing interest

The authors declare that they have no known competing financial interests or personal relationships that could have appeared to influence the work reported in this paper.

## Acknowledgment

This study was fully granted by the Scientific and Technological Research Council of Turkey (TUBİTAK) under Project No: 115M363. TUBİTAK's financial support is greatly appreciated.

## References

[1] A. Özacar, N. Kaymakcı, S. Akkar, A. Azari, A. Sandıkkaya, Ö. Kale, B.Ö. Ay, 23 Ekim 2011 Mw 7.2 Van depremi sismik ve yapısal hasara ilişkin saha gözlemleri, Rep. No: METU/EERC 402 (2011) 2011–2014.
[2] T.E. Alqado, G. Nikolakopoulos, L. Dritsas, Semi-active control of flexible structures using closed-loop input shaping techniques, Struct. Contr. Health Monit. 24 (5) (2017), e1913.
[3] S. Elias, V. Matsagar, Wind response control of tall buildings with a tuned mass damper, Journal of Building Engineering 15 (2018) 51–60.
[4] H. Jarrahi, A. Asadi, M. Khatibinia, S. Etedali, Optimal design of rotational friction dampers for improving seismic performance of inelastic structures, Journal of Building Engineering 27 (2020) 100960.
[5] C.A. Martínez, O. Curadelli, M.E. Compagnoni, Optimal design of passive viscous damping systems for buildings under seismic excitation, J. Constr. Steel Res. 90 (2013) 253–264.
[6] J.D. Marshall, F.A. Charney, Seismic response of steel frame structures with hybrid passive control systems, Earthq. Eng. Struct. Dynam. 41 (4) (2012) 715–733.
[7] P. Martinelli, M.G. Mulas, An innovative passive control technique for industrial precast frames, Eng. Struct. 32 (4) (2010) 1123–1132.
[8] K. Hiramoto, Cooperative control method of active and Semiactive control: new framework for vibration control, Math. Probl Eng. 2014 (2014).
[9] Y. Chae, J.M. Ricles, R. Sause, Large-scale experimental studies of structural control algorithms for structures with magnetorheological dampers using real-time hybrid simulation, J. Struct. Eng. 139 (7) (2013) 1215–1226.
[10] S. Cetin, E. Zergeroglu, S. Sivrioglu, I. Yuksek, A new semiactive nonlinear adaptive controller for structures using MR damper: design and experimental validation, Nonlinear Dynam. 66 (4) (2011) 731–743.
[11] H.J. Lee, H.J. Jung, S.J. Moon, S.K. Lee, E.C. Park, K.W. Min, Experimental investigation of MR damper-based semiactive control algorithms for full-scale five-story steel frame building, J. Intell. Mater. Syst. Struct. 21 (10) (2010) 1025–1037.
[12] D. Das, T.K. Datta, A. Madan, Seismic control of building frames using MR damper, in: The 14 Th World Conference on Earthquake Engineering, 2008, pp. 12–17.
[13] Y. Choe, November). Intelligent pid controller and its application to structural vibration mitigation with mr damper, in: 2016 14th International Conference on Control, Automation, Robotics and Vision (ICARCV), IEEE, 2016, pp. 1–6.
[14] S.J. Dyke, B.F. Spencer Jr., M.K. Sain, J.D. Carlson, Modeling and control of magnetorheological dampers for seismic response reduction, Smart Mater. Struct. 5 (5) (1996) 565.
[15] R. Guclu, Sliding mode and PID control of a structural system against earthquake, Math. Comput. Model. 44 (1–2) (2006) 210–217.
[16] C.O. Saglam, E.A. Baran, A.O. Nergiz, A. Sabanovic, Model following control with discrete time SMC for time-delayed bilateral control systems, in: 2011 IEEE International Conference on Mechatronics, IEEE, 2011, April, pp. 997–1002.
[17] Q.P. Ha, M.T. Nguyen, J. Li, N.M. Kwok, Smart structures with current-driven MR dampers: modeling and second-order sliding mode control, IEEE ASME Trans. Mechatron. 18 (6) (2013) 1702–1712.
[18] L.M. Jansen, S.J. Dyke, Semiactive control strategies for MR dampers: comparative study, J. Eng. Mech. 126 (8) (2000) 795–803.
[19] I.H. Vadtala, D.P. Soni, D.G. Panchal, Semi-active control of a benchmark building using neuro-inverse dynamics of MR damper, Procedia Engineering 51 (2013) 45–54.
[20] M. Bitaraf, O.E. Ozbulut, S. Hurlebaus, L. Barroso, Application of semi-active control strategies for seismic protection of buildings with MR dampers, Eng. Struct. 32 (10) (2010) 3040–3047.
[21] A. Bayraktar, T. Turker, M. Ozcan, M. Akkose, S. Adanur, S. Ates, Yapısal Hasarların Deneysel Ve Operasyonal Modal Analiz Yöntemleriyle Belirlenmesi Project No: 106M038, 2009.
[22] R.C. Hibbeler, T. Kiang, Structural Analysis, Pearson Prentice Hall, Upper Saddle River, 2015.
[23] Q. Zhou, W. lian Qu, Two mechanical models for magnetorheological damper and corresponding test verification, Journal of Earthquake Engineering and Engineering Vibration 22 (4) (2002) 144–150. Aug. 2002.
[24] R. Jiménez, L. Álvarez-Icaza, LuGre friction model for a magnetorheological damper, Struct. Contr. Health Monit. 12 (1) (2005) 91–116.
[25] N.M. Kwok, Q.P. Ha, T.H. Nguyen, J. Li, B. Samali, A novel hysteretic model for magnetorheological fluid dampers and parameter identification using particle swarm optimization, Sensor Actuator Phys. 132 (2) (2006) 441–451.
[26] D. Guo, H. Hu, Nonlinear stiffness of a magneto-rheological damper, Nonlinear Dynam. 40 (3) (2005) 241–249.
[27] M. Zhu, X. Wei, L. Jia, Building an inverse model of MR damper based on Dahl model, in: 17th International IEEE Conference on Intelligent Transportation Systems (ITSC), IEEE, 2014, October, pp. 1148–1153.
[28] L.H. Zong, X.L. Gong, C.Y. Guo, S.H. Xuan, Inverse neuro-fuzzy MR damper model and its application in vibration control of vehicle suspension system, Veh. Syst. Dyn. 50 (7) (2012) 1025–1041.
[29] P.Q. Xia, An inverse model of MR damper using optimal neural network and system identification, J. Sound Vib. 266 (5) (2003) 1009–1023.

[30] C.C. Chang, L. Zhou, Neural network emulation of inverse dynamics for a magnetorheological damper, J. Struct. Eng. 128 (2) (2002) 231–239.
[31] S. Bhowmik, J.B. Høgsberg, F. Weber, Neural Network modeling of forward and inverse behavior of rotary MR damper, in: 23rd Nordic Seminar on Computation Mechanics (NSCM23), Stockholm, Sweden, 2010, October.
[32] W. Liu, W.K. Shi, D.W. Liu, T.Y. Yan, Experimental modeling of magneto-rheological damper and PID neural network controller design, in: *2010* Sixth International Conference on Natural Computation, vol. 4, IEEE, 2010, August, pp. 1674–1678.
[33] H.H. Zhang, C.R. Liao, W.M. Chen, Modeling of magneto-rheological damper with neural network, J. China Univ. Min. Technol. 16 (1) (2006) 50–52.
[34] H.C. Cho, M.S. Fadali, M.S. Saiidi, K.S. Lee, Neural network active control of structures with earthquake excitation, Int. J. Contr. Autom. Syst. 3 (2) (2005) 202–210.
[35] J.S. Smith, B. Wu, B.M. Wilamowski, Neural network training with Levenberg–Marquardt and adaptable weight compression, IEEE transactions on neural networks and learning systems 30 (2) (2018) 580–587.
[36] Y. Ohtori, R.E. Christenson, B.F. Spencer Jr., S.J. Dyke, Benchmark control problems for seismically excited nonlinear buildings, J. Eng. Mech. 130 (4) (2004) 366–385.
[37] F.A. Charney, Seismic Loads: Guide to the Seismic Load Provisions of ASCE 7-10, American Society of Civil Engineers, 2015, February.